

# Resonant Auger Decay in Benzene

Published as part of *The Journal of Physical Chemistry A* special issue “Trygve Helgaker Festschrift”.

Nayanthara K. Jayadev, Thomas-C. Jagau, and Anna I. Krylov\*



Cite This: *J. Phys. Chem. A* 2025, 129, 733–743



Read Online

ACCESS |



Metrics & More

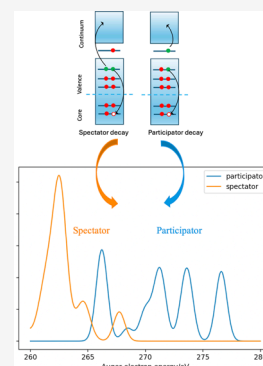


Article Recommendations



Supporting Information

**ABSTRACT:** We present ab initio calculations of the resonant Auger spectrum of benzene. In the resonant process, Auger decay ensues following the excitation of a core-level electron to a virtual orbital. Hence, resonant Auger decay gives rise to higher-energy Auger electrons compared to nonresonant decay. We apply equation-of-motion coupled-cluster (EOM-CC) methods to compute the spectrum in order to explain the main features in the experimental spectrum and to assess the capability and limitations of the available theoretical approaches. The results indicate that participator decay can be well described with the Feshbach–Fano approach based on EOM-CC wave functions in the singles and doubles (SD) approximation, but spectator decay is more difficult to describe. This is because the target states of spectator decay are doubly excited, resulting in the need to include triple excitations in the EOM-CC wave function. Resonant Auger decay in benzene is thus a challenging test case for EOM-CC theory. We examine the performance of different noniterative triple corrections to EOM-IP-CCSD and our numerical results highlight the need to include triple excitations iteratively.



## 1. INTRODUCTION

Auger decay is a nonradiative process in which a core-vacancy state decays by filling the hole and ejecting a second electron. It is a consequence of the metastable nature of highly energetic core-vacancy states located well above the ionization onset. Depending on whether the initial state is core-excited or core-ionized, one can distinguish between resonant and non-resonant Auger decay, as illustrated in Figure 1. In the former, the final states are singly ionized and in the latter doubly ionized.

Figure 1 also shows that resonant Auger decay can be further classified as participator or spectator decay depending on whether the initially excited electron takes part in the decay. Regular Auger decay takes place when the excitation energy

exceeds the core ionization energy whereas the resonant Auger process takes place when the excitation energy is below the ionization threshold of the respective core.

Auger processes accompany many—if not all—X-ray induced processes.<sup>1</sup> Practical uses of Auger electrons include analytical techniques for surfaces,<sup>2–4</sup> materials,<sup>5</sup> nanostructures,<sup>6–8</sup> and molecules.<sup>9–12</sup> In addition, Auger electrons are also used for precision cancer treatments.<sup>13–17</sup> As with other spectroscopies, theoretical modeling helps to interpret the experimental spectra in terms of essential details of electronic structure. The positions of the peaks in an Auger spectrum are the energies of the Auger electrons, given by the energy differences between the initial core-hole state and the final states. The intensities of the individual peaks are proportional to the respective rates of decay, which are in turn proportional to the partial widths of the core-hole state. As per Figure 1, participator decay should result in faster Auger electrons relative to nonresonant and spectator decay, whereas the spectator decay is expected to contribute to the lower-energy part of the Auger spectrum.

Ab initio calculations of Auger spectra are challenging because of the difficulties with computing core-vacancy states due to their metastable nature. Additional complications arise

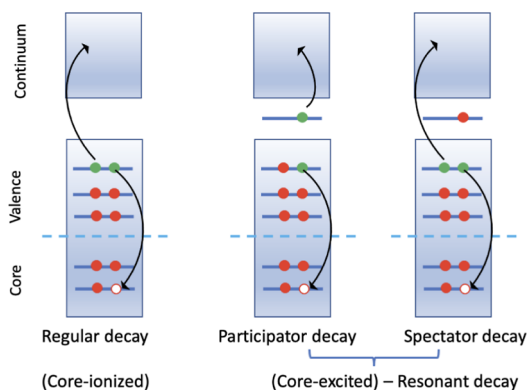


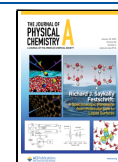
Figure 1. Different types of Auger decay.

Received: October 27, 2024

Revised: December 11, 2024

Accepted: December 16, 2024

Published: January 13, 2025



due to the large number of decay channels and the open-shell character of the final states.

In early theoretical work on molecular Auger decay, the decay rates were assumed to be identical for all target states of a given multiplicity.<sup>18,19</sup> The results indicated that for polyatomic molecules, nonresonant Auger spectra could be reasonably well described by using the density of final states, provided that the contributions of triplet decay channels are scaled down relative to singlet channels.

In a more rigorous approach, the decay rates are computed explicitly. One possible technique is the Feshbach–Fano method in which the Hilbert space is partitioned into bound and continuum configurations.<sup>20–22</sup> The core–valence separation is commonly used to define the bound part of the Hilbert space.<sup>23–27</sup> For the treatment of the continuum part, a great variety of methods have been proposed. For example, Stieltjes imaging<sup>28,29</sup> was employed on top of the algebraic diagrammatic construction (ADC) approach<sup>30</sup> to evaluate partial widths, which were then normalized to sum up to the correct total width.<sup>31,32</sup> Recently, Kolorenc and Averbukh introduced the Fano–ADC(2,2) method,<sup>33</sup> which provides an improved description of the initial and final states, and is also useful for modeling double Auger decay.<sup>34</sup>

Whereas Stieltjes imaging treats the continuum wave functions implicitly, it is also possible to construct them explicitly, for example, by using the one-center approximation<sup>35–38</sup> or by solving a one-electron radial Schrödinger equation with spherical continuum wave functions.<sup>39,40</sup> Time-dependent studies of resonant Auger decay,<sup>41</sup> including the investigation of core-excited CO by Demekhin and Cederbaum,<sup>42</sup> are also noteworthy.

Recently, two new approaches for computing decay rates of core-hole states were introduced—one based on the Feshbach–Fano formalism<sup>43</sup> and another based on the complex basis functions (CBF) method.<sup>44–47</sup> Both techniques were implemented using the equation-of-motion coupled-cluster (EOM-CC) ansatz<sup>48</sup> for describing initial core-hole and final valence-ionized states and tested on atoms and small molecules for which highly reliable partial decay widths and well-resolved Auger spectra are available.<sup>46,47,49–53</sup>

These two CC/EOM-CC based techniques were also applied to compute the nonresonant Auger spectrum of benzene,<sup>54</sup> resulting in a remarkable agreement between the two fundamentally different approaches for treating the continuum. The comparison with the experiment was less straightforward because three experimental studies<sup>55–57</sup> reported Auger spectra of benzene that did not align even after applying a global shift. However, the computations captured the general shape of the spectrum well, with differences of the same magnitude as the discrepancies between the experimental spectra.

In this contribution, we extend our study of Auger decay in benzene to the resonant process. Both resonant and nonresonant Auger spectra of benzene were reported by Rennie et al., who measured absolute photoabsorption cross sections of benzene using synchrotron radiation.<sup>56</sup> Resonant and regular Auger spectra were measured at the main features of the photoabsorption spectrum of benzene, including the most intense  $1s_C \rightarrow \pi^*$  resonance. Figure 2 shows these experimental Auger spectra. As expected, the resonant spectrum features several higher-energy peaks relative to the nonresonant spectrum. We will discuss the experimental spectra in more detail below, after reviewing the electronic

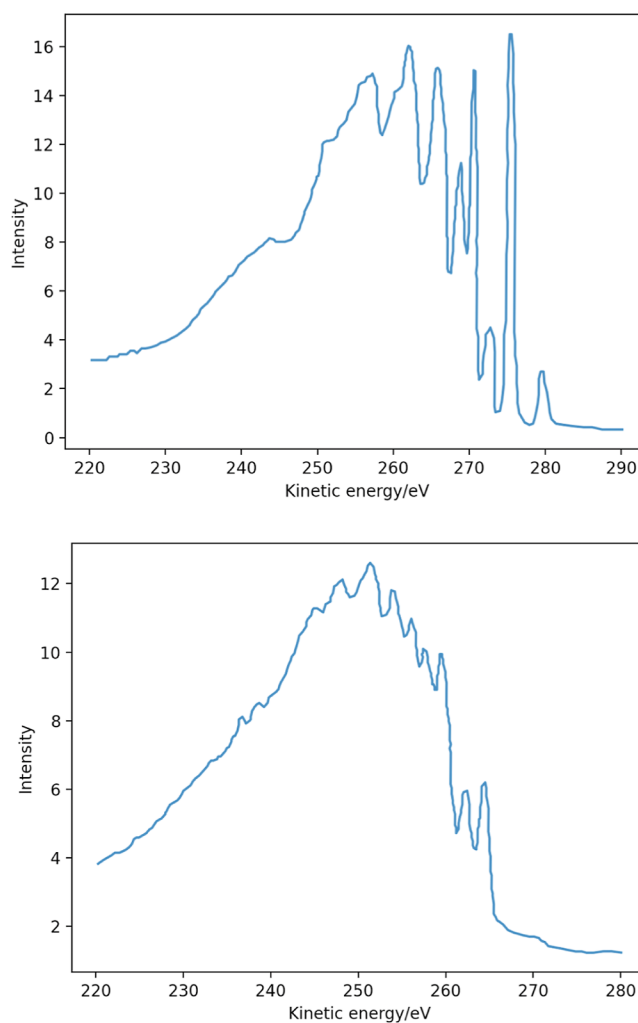


**Figure 2.** Auger spectra of benzene measured at two different X-ray energies (digitized from ref 56). Top panel: 285 eV. Bottom panel: 390 eV (sudden limit).

structure and the X-ray absorption spectrum (XAS) of benzene.

The structure of the paper is as follows. Section 2 describes the computational methods. The numerical results and a comparison with the experiment are presented in Section 3. Our concluding remarks are given in Section 4.

## 2. COMPUTATIONAL DETAILS

We computed the Auger spectrum using the Feshbach–Fano approach combined with EOM-CC wave functions in the singles and doubles approximation (EOM-CCSD) as devised by Skomorowski and Krylov.<sup>43,49</sup> The initial states of the resonant Auger decay process, in which one core electron is excited to a virtual orbital, were computed using CVS-EOM-EE-CCSD using the frozen-core CVS (fc-CVS) framework.<sup>25–27</sup> The final states, i.e., the decay channels, were computed using EOM-IP-CCSD; the core electrons in the carbon K-shells were frozen in these calculations.

As shown in Figure 3, in the case of participator and spectator decay the decay channels correspond to 1-hole (1h) and 2-hole-1-particle (2h1p) EOM-IP-CC states, respectively. This means that the spectator decay channels are not described well within the EOM-CCSD approximation. To account for triple excitations, we carried out EOM-IP-CCSD(ft)<sup>58,59</sup> and

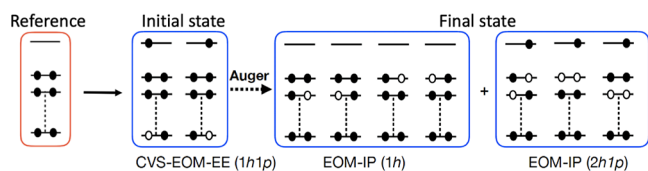


**Figure 3.** Initial and final states in resonant Auger decay can be computed with CVS-EOM-EE-CCSD and EOM-IP-CCSD, respectively.

EOM-IP-CCSD(T)(a)\* calculations.<sup>60,61</sup> In the former method, a correction to the EOM-CCSD energy is computed using biorthogonal second-order Rayleigh–Schrödinger perturbation theory applied to the similarity-transformed Hamiltonian and treating the EOM-CCSD states as zero-order states.<sup>58,59</sup> In the EOM-IP-CCSD(T)(a)\* method,<sup>60,61</sup> the correction is applied to the EOM-CC similarity-transformed Hamiltonian, meaning that the effect of triple excitations is included not only in the energy but also in the EOM amplitudes. The benchmarks<sup>61</sup> indicated that EOM-IP-CCSD(T)(a)\* generally affords better results than EOM-IP-CCSD(fT).

In all EOM-CC calculations, the closed-shell ground state of benzene was used as the reference state.

The fully uncontracted 6-311(2+,+)G\*\* basis set, denoted as u6-311(2+,+)G\*\*, was used in all EOM-CCSD calculations.<sup>62,63</sup> We used the same basis set for EOM-IP-CCSD(fT) and EOM-IP-CCSD(T)(a)\* calculations. However, due to convergence issues in the EOM-IP-CCSD(T)(a)\* calculations, we were unable to compute a sufficient number of  $2h1p$  states. Thus, we carried out additional EOM-IP-CCSD(T)(a)\* calculations for the missing states using the 6-311(+)G\* basis.

The continuum orbital was treated as a plane wave in the calculations of the decay widths. The  $k$ -vector integration in these calculations was carried out using Lebedev quadrature. We note that calculations with the default grid of order 5 yield partial widths that break symmetry-imposed constraints.<sup>54</sup> Hence, we computed the resonant Auger spectrum of benzene with a tighter integration grid of order 17; the difference between the spectra obtained with the two grids is shown in the Supporting Information. The Auger spectra were generated from the computed energies and decay widths convoluted with a Gaussian function with a fixed full width at half-maximum equal to 1.15 eV.

All calculations were carried out using the Q-Chem package<sup>64,65</sup> at the equilibrium structure of benzene optimized with RI-MP2/cc-pVTZ; Cartesian coordinates are given in the Supporting Information.

### 3. RESULTS AND DISCUSSION

**3.1. Molecular Orbitals of Benzene.** The molecular orbital (MO) diagram of benzene is shown in Figure 4. Benzene belongs to the non-Abelian point group  $D_{6h}$ . Since most quantum chemistry packages, including Q-Chem, use Abelian groups, we use in the discussion below the irreducible representations of the Abelian subgroup  $D_{2h}$  for the electronic states and MOs. The electronic configuration of the core electrons is

$$(1a_g)^2(1b_{3u})^2(1b_{2u})^2(2a_g)^2(1b_{1g})^2(2b_{3u})^2 \quad (1)$$

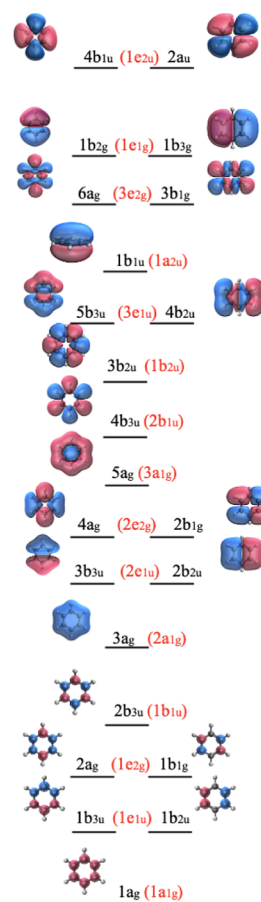


**Figure 4.** Molecular orbital diagram of benzene. Irreducible representations are given for the full point group  $D_{6h}$  (in red) using Mulliken's convention<sup>66</sup> and for the largest Abelian subgroup  $D_{2h}$  (in black) using Q-Chem's convention.<sup>67</sup> The  $\pi^*$   $1e_{2u}$  orbitals are the two lowest unoccupied molecular orbitals (LUMOs).

corresponding to the six  $1s_C$  orbitals. The  $1b_{3u}$  and  $1b_{2u}$  orbitals as well as the  $2a_g$  and  $1b_{1g}$  orbitals are degenerate and form the  $1e_{1u}$  and  $1e_{2g}$  shells, respectively, in the full point group.

**3.2. X-ray Absorption Spectrum of Benzene.** To understand the resonant Auger spectrum of benzene, we begin by reviewing its XAS spectrum. XAS probes core-excited states, which are the initial states of resonant Auger decay. Figure 5 shows the XAS spectrum of benzene computed by Nanda et al.<sup>68,69</sup> The positions and relative intensities of the main peaks agree with the experimental spectrum after applying a redshift of 0.8 eV.

Figure 5 also shows the leading natural transition orbitals (NTOs).<sup>70,71</sup> According to the NTOs, the peak A in the XAS spectrum originates from  $1s_C \rightarrow \pi^*$  transitions and the doubly degenerate peak B originates from  $1s_C \rightarrow \text{Ry}(B_{2u}/B_{3u})$  transitions. The NTO analysis further reveals that the excitations that give rise to peak A create a hole in the  $1a_g$  and  $1b_{1g}$  core orbitals, whereas the excitations that correspond to peak B create holes in the  $1b_{2u}/1b_{3u}$  and  $1a_g$  orbitals.

In the Supporting Information (Figure S1 and Table S1) we show the XAS transitions that cover the relevant energy range as well as excitation energies and oscillator strengths computed in the fully uncontracted 6-311(2+,+)G\*\* basis set. The results are similar to those computed in the partially uncontracted 6-311(2+,+)G\*\* basis set used in ref 68.

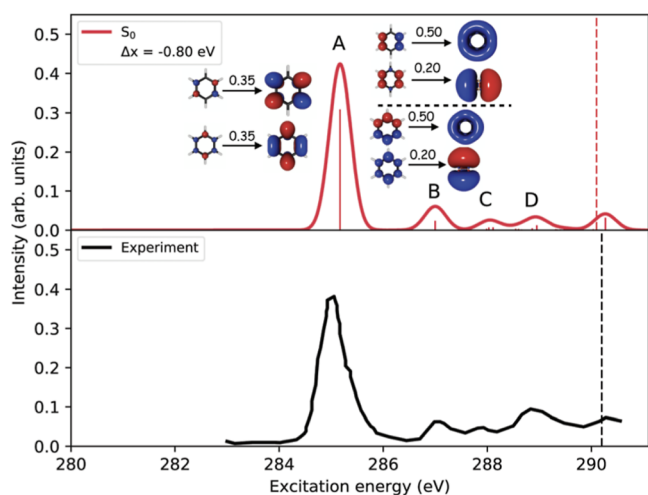


**Figure 5.** XAS spectrum of benzene computed with CVS-EOM-EE-CCSD in the 6-311(2+,+)G\*\* basis set with uncontracted carbon core. Reproduced with permission from ref 68; Copyright: Royal Society of Chemistry.

As discussed in the introduction, we compare our results to the experimental spectra by Rennie et al.<sup>56</sup> (see Figure 2). They reported the XAS of benzene in the range from 285 eV to beyond the  $1s_C$  threshold at 290.42 eV. In agreement with other reported XAS of benzene,<sup>72,73</sup> the by far most prominent feature is the  $1s_C \rightarrow \pi^*$  excitation at around 285 eV, which is termed peak A in ref 68.

Figure 2 shows the Auger spectrum measured at 285 eV, where the  $1s_C \rightarrow \pi^*$  resonance is located, as well as in sudden limit conditions at 390 eV, i.e., way above the ionization threshold.<sup>56</sup> The Auger spectrum measured at 390 eV corresponds to regular Auger decay, which we discussed in ref 54. Here, we focus on the spectrum measured at 285 eV, which corresponds to resonant Auger decay following excitation to the  $1s_C \rightarrow \pi^*$  state (peak A). This state, which has  $1B_{1u}$  symmetry in the  $D_{2h}$  subgroup, is the initial state in our calculations of resonant Auger decay. For comparison, we also computed Auger spectra for decay of the  $1B_{2u}/1B_{3u}$  state, corresponding to peak B in the XAS. Unfortunately, Rennie et al.<sup>56</sup> did not report experimental Auger spectra with an excitation energy corresponding to peak B.

**3.3. EOM-IP-CCSD Calculations of the Decay Channels.** Table 1 lists the ionization energies (IEs) of the lowest ionized states of benzene computed with EOM-IP-CCSD. The EOM-IP amplitudes clearly identify the decay channels as corresponding to either participator or spectator decay (see Figure 3). The  $1h$  states, characterized by the large square norm of  $R_1$ , correspond to participator decay and the  $2h1p$  states, characterized by the large square norm of  $R_2$ , correspond to spectator decay.

According to Table 1, the  $1h$  states give rise to the lower IE part of the Auger spectrum, i.e., the part with higher Auger electron energy. The  $2h1p$  spectator decay channels, derived by the removal of a valence electron and an accompanying excitation to the LUMO, give rise to lower-energy Auger electrons. Table 1 shows several spectator decay channels in which two electrons are removed from higher-lying occupied orbitals and one is placed in a low-lying virtual orbital. The analysis of the wave function reveals the multiconfigurational character of the  $2h1p$  states.

**Table 1. IEs and Wavefunction Composition in Terms of the Leading Amplitudes of the Lowest Ionized States of Benzene Computed with EOM-IP-CCSD/u6-311(2+,+)G\*\*<sup>a</sup>**

state	composition	energy (eV)	$R_1^2$	$R_2^2$
$2B_{2g}/2B_{3g}$	$1b_{2g}^{-1} (0.97)/1b_{3g}^{-1} (0.97)$	9.23	0.94	0.06
$2A_g/2B_{1g}$	$6a_g^{-1} (0.96)/3b_{1g}^{-1} (0.96)$	12.12	0.93	0.07
$2B_{1u}$	$1b_{1u}^{-1} (0.94)$	12.55	0.90	0.10
$2B_{2u}/2B_{3u}$	$4b_{2u}^{-1} (0.96)/5b_{3u}^{-1} (0.96)$	14.41	0.92	0.08
$2B_{2u}$	$3b_{2u}^{-1} (0.96)$	14.82	0.91	0.09
$2B_{3u}$	$4b_{3u}^{-1} (0.96)$	15.83	0.90	0.10
$2A_g$	$5a_g^{-1} (0.94)$	17.38	0.89	0.11
$2A_g/2B_{1g}$	$4a_g^{-1} (0.92)/2b_{1g}^{-1} (0.92)$	19.62	0.86	0.14
$2A_u/2B_{1u}$	$1b_{2g}^{-1}1b_{3g}^{-1}4b_{1u}^{-1} (0.50), 1b_{2g}^{-1}1b_{3g}^{-1}6b_{1u}^{-1} (0.23)/1b_{2g}^{-1}1b_{3g}^{-1}2a_u^{-1} (0.50), 1b_{2g}^{-1}1b_{3g}^{-1}3a_u^{-1} (0.50)$	17.56	0.00	1.00
$2A_u/2B_{1u}$	$1b_{2g}^{-1}2a_u^{-1} (0.66), 1b_{2g}^{-1}1b_{3g}^{-1}4b_{1u}^{-1} (0.41)/1b_{2g}^{-1}4b_{1u}^{-1} (0.66), 1b_{2g}^{-1}1b_{3g}^{-1}2a_u^{-1} (0.41)$	18.10	0.00	1.00
$2A_u/2B_{1u}$	$1b_{2g}^{-1}2a_u^{-1} (0.60), 1b_{2g}^{-1}1b_{3g}^{-1}4b_{1u}^{-1} (0.43)/1b_{2g}^{-1}4b_{1u}^{-1} (0.60), 1b_{2g}^{-1}1b_{3g}^{-1}2a_u^{-1} (0.43)$	20.27	0.00	1.00
$2B_{3g}$	$1b_{3g}^{-1}1b_{2g}^{-1}6b_{1u}^{-1} (0.31), 1b_{2g}^{-1}1b_{1u}^{-1}4b_{1u}^{-1} (0.29), 1b_{2g}^{-1}1b_{1u}^{-1}2a_u^{-1} (0.29)$	19.88	0.00	1.00
$2B_{2g}$	$1b_{3g}^{-1}1b_{1u}^{-1}2a_u^{-1} (0.36), 1b_{2g}^{-1}1b_{1u}^{-1}4b_{1u}^{-1} (0.36)$	20.00	0.00	1.00
$2B_{2g}/2B_{3g}$	$1b_{3g}^{-1}1b_{1u}^{-1}2a_u^{-1} (0.36), 1b_{2g}^{-1}1b_{1u}^{-1}4b_{1u}^{-1} (0.36)/1b_{2g}^{-1}1b_{1u}^{-1}2a_u^{-1} (0.36), 1b_{3g}^{-1}1b_{1u}^{-1}4b_{1u}^{-1} (0.36)$	21.45	0.00	1.00

<sup>a</sup>The square norms of  $R_1^2$  and  $R_2^2$  distinguish  $1h$  and  $2h1p$  states.

**3.4. Resonant Auger Decay Widths.** Tables 2 and 3 show the Auger electron energies and partial widths of the major decay channels of the  $1B_{1u}$  and  $1B_{2u}$  core-excited states of benzene computed with EOM-CCSD; the results for the  $1B_{3u}$  state (which is degenerate with  $1B_{2u}$ ) are given in the Supporting Information. The  $1B_{1u}$  state gives rise to larger decay widths relative to the  $1B_{2u}/1B_{3u}$  states. Almost all participator decay channels ( $1h$  channels) of the  $1B_{1u}$  state have substantial partial width above 1 meV, leading to faster decay and, consequently, a higher probability of decay of the metastable core-excited state into these channels. The partial decay widths of the spectator decay channels ( $2h1p$  channels) are smaller. This may be attributed to the stronger Coulomb interaction of the valence electrons with the core; for example, for autoionizing Rydberg states, it is well established that weaker interaction with the molecular core results in lower decay width.<sup>74–76</sup> However, our results might also be affected by an insufficient description of the  $2h1p$  states. Notably, our calculations identified a large number of spectator decay channels, such that their combined width is substantial.

Previous investigations showed that the branching ratio between spectator and participator decay can vary significantly and is sensitive to the molecular electronic structure; for example, in  $CH_4$  and  $CF_4$  participator decay contributes no more than 6% to the total decay width<sup>77,78</sup> whereas that number amounts to 21% for the C-edge of CO.<sup>79</sup> We thus cannot say with certainty whether the dominance of the participator channels in benzene found by our calculations is real or an artifact due to an insufficient description of the electronic structure.

**3.5. Resonant Auger Spectrum of Benzene.** Figure 6 shows the contributions of  $1h$  states and  $2h1p$  states to the

**Table 2. Auger Electron Energies (in eV) and Partial Decay Widths (in meV) for the Main Channels in Resonant Auger Decay of the Core-Excited  $^1B_{1u}$  State of Benzene**

decay channel	transition	energy	width	
$^2A_g(6a_g^{-1})/{}^2B_{1g}(3b_{1g}^{-1})$	$B_{1u}/A_u$	273.71	1.07	participator
$^2A_g(5a_g^{-1})$	$B_{1u}$	268.45	0.49	participator
$^2A_g(4a_g^{-1})/{}^2B_{1g}(2b_{1g}^{-1})$	$B_{1u}/A_u$	266.21	1.76	participator
$^2B_{2g}(1b_{2g}^{-1})/{}^2B_{3g}(1b_{3g}^{-1})$	$B_{3u}/B_{2u}$	276.60	1.34	participator
$^2B_{2u}(4b_{2u}^{-1})/{}^2B_{3u}(5b_{3u}^{-1})$	$B_{3g}/B_{2g}$	271.42	0.85	participator
$^2B_{2u}(3b_{2u}^{-1})$	$B_{3g}$	271.01	1.33	participator
$^2B_{3u}(4b_{3u}^{-1})$	$B_{2g}$	270.00	1.18	participator
$^2A_g(1b_{2g}^{-1}5b_{3u}^{-1}4b_{1u}^{-1}, 1b_{3g}^{-1}5b_{3u}^{-1}2a_u^{-1})/{}^2B_{1g}(1b_{3g}^{-1}4b_{2u}^{-1}2a_u^{-1}, 1b_{2g}^{-1}4b_{2u}^{-1}4b_{1u}^{-1})$	$B_{1u}/A_u$	262.47	0.42	spectator
$^2B_{2g}(1b_{2g}^{-1}1b_{1u}^{-1}4b_{1u}^{-1}, 1b_{3g}^{-1}1b_{1u}^{-1}2a_u^{-1})$	$B_{3u}$	263.21	0.58	spectator
$^2B_{2g}(1b_{3g}^{-1}1b_{1u}^{-1}2a_u^{-1}, 1b_{2g}^{-1}1b_{1u}^{-1}4b_{1u}^{-1}, 1b_{2g}^{-1}6b_{2g}^{-1}, 1b_{3g}^{-1}6b_{2g}^{-1})$	$B_{3u}$	262.87	0.55	spectator
$^2B_{2g}(1b_{2g}^{-1}6b_{2g}^{-1}, 1b_{3g}^{-1}6b_{2g}^{-1})/{}^2B_{3g}(1b_{2g}^{-1}1b_{3g}^{-1}6b_{2g}^{-1})$	$B_{3u}/B_{2u}$	262.17	0.33	spectator
$^2A_u(1b_{3g}^{-1}2a_u^{-1}, 1b_{3g}^{-1}1b_{2g}^{-1}4b_{1u}^{-1})/{}^2B_{1u}(1b_{2g}^{-1}4b_{1u}^{-1}, 1b_{2g}^{-1}1b_{3g}^{-1}2a_u^{-1})$	$B_{1g}/A_g$	267.73	0.56	spectator
$^2B_{1u}(1b_{3g}^{-1}1b_{2g}^{-1}2a_u^{-1}, 1b_{2g}^{-1}4b_{1u}^{-1}, 1b_{3g}^{-1}4b_{1u}^{-1})$	$A_g$	264.21	0.75	spectator
$^2B_{2u}(1b_{2g}^{-1}3b_{1u}^{-1}4b_{1u}^{-1}, 1b_{3g}^{-1}3b_{1u}^{-1}2a_u^{-1})/{}^2B_{3u}(1b_{3g}^{-1}6a_g^{-1}2a_u^{-1}, 1b_{2g}^{-1}6a_g^{-1}4b_{1u}^{-1})$	$B_{3g}/B_{2g}$	264.80	0.52	spectator
$^2B_{2u}(2b_{2u}^{-1}, 1b_{2g}^{-1}6a_g^{-1}2a_u^{-1}, 1b_{2g}^{-1}3b_{1u}^{-1}4b_{1u}^{-1})/{}^2B_{3u}(3b_{3u}^{-1}, 1b_{3g}^{-1}3b_{1u}^{-1}4b_{1u}^{-1}, 1b_{3g}^{-1}6a_g^{-1}2a_u^{-1})$	$B_{3g}/B_{2g}$	262.50	1.12	spectator

**Table 3. Auger Electron Energies (in eV) and Partial Decay Widths (in meV) for the Main Channels in Resonant Auger Decay of the Core-Excited  $^1B_{2u}$  State of Benzene**

decay channel	transition	energy	width	
$^2A_g(6a_g^{-1})$	$B_{2u}$	275.54	0.56	participator
$^2B_{1g}(3b_{1g}^{-1})$	$B_{3u}$	275.54	0.38	participator
$^2A_g(5a_g^{-1})$	$B_{2u}$	270.29	0.29	participator
$^2A_g(4a_g^{-1})$	$B_{2u}$	268.05	0.32	participator
$^2B_{1g}(2b_{1g}^{-1})$	$B_{3u}$	268.05	0.28	participator
$^2B_{2g}(1b_{2g}^{-1})$	$A_u$	278.43	0.22	participator
$^2B_{3g}(1b_{3g}^{-1})$	$B_{1u}$	278.43	0.64	participator
$^2B_{1u}(1b_{1u}^{-1})$	$B_{3g}$	275.11	0.33	participator
$^2B_{2u}(4b_{2u}^{-1})$	$A_g$	273.25	0.70	participator
$^2B_{3u}(5b_{3u}^{-1})$	$B_{1g}$	273.25	0.31	participator
$^2B_{2u}(3b_{2u}^{-1})$	$A_g$	272.85	0.59	participator
$^2B_{3u}(4b_{3u}^{-1})$	$B_{1g}$	271.83	0.11	participator
$^2A_g(1b_{2g}^{-1}13a_g^{-1}, 1b_{3g}^{-1}13a_g^{-1}, 1b_{2g}^{-1}9a_g^{-1}, 1b_{3g}^{-1}9a_g^{-1})$	$B_{2u}$	264.69	0.32	spectator
$^2A_g(1b_{2g}^{-1}13a_g^{-1}, 1b_{3g}^{-1}13a_g^{-1}, 1b_{2g}^{-1}9a_g^{-1}, 1b_{3g}^{-1}9a_g^{-1})$	$B_{2u}$	264.50	0.13	spectator
$^2B_{1g}(1b_{3g}^{-1}1b_{2g}^{-1}13a_g^{-1}, 1b_{3g}^{-1}1b_{2g}^{-1}9a_g^{-1})$	$B_{3u}$	264.50	0.52	spectator
$^2A_g(1b_{2g}^{-1}13a_g^{-1}, 1b_{3g}^{-1}13a_g^{-1}, 1b_{2g}^{-1}11a_g^{-1}, 1b_{3g}^{-1}11a_g^{-1})$	$B_{2u}$	263.44	0.06	spectator
$^2B_{1g}(1b_{3g}^{-1}1b_{2g}^{-1}13a_g^{-1}, 1b_{3g}^{-1}1b_{2g}^{-1}11a_g^{-1})$	$B_{3u}$	263.44	0.23	spectator
$^2B_{2g}(1b_{2g}^{-1}6a_g^{-1}11a_g^{-1}, 1b_{3g}^{-1}3b_{1g}^{-1}11a_g^{-1})$	$A_u$	262.16	0.30	spectator
$^2B_{2g}(1b_{2g}^{-1}6a_g^{-1}11a_g^{-1}, 1b_{3g}^{-1}3b_{1g}^{-1}11a_g^{-1}, 1b_{2g}^{-1}6a_g^{-1}15a_g^{-1}, 1b_{3g}^{-1}3b_{1g}^{-1}15a_g^{-1})$	$A_u$	262.31	0.14	spectator
$^2B_{3g}(1b_{3g}^{-1}6a_g^{-1}11a_g^{-1}, 1b_{2g}^{-1}3b_{1g}^{-1}11a_g^{-1}, 1b_{3g}^{-1}6a_g^{-1}15a_g^{-1}, 1b_{2g}^{-1}3b_{1g}^{-1}15a_g^{-1})$	$B_{1u}$	262.31	0.16	spectator
$^2A_u(3b_{1g}^{-1}1b_{3g}^{-1}8b_{2u}^{-1}, 3b_{1g}^{-1}1b_{3g}^{-1}10b_{2u}^{-1})$	$B_{2g}$	261.65	0.34	spectator
$^2B_{1u}(6a_g^{-1}1b_{2g}^{-1}9b_{3u}^{-1}, 6a_g^{-1}1b_{2g}^{-1}11b_{3u}^{-1})$	$B_{3g}$	261.65	0.14	spectator
$^2B_{1u}(5b_{3u}^{-1}1b_{2g}^{-1}11a_g^{-1}, 4b_{2u}^{-1}1b_{3g}^{-1}11a_g^{-1})$	$B_{3g}$	261.51	0.23	spectator
$^2B_{2u}(2b_{2u}^{-1}, 1b_{2g}^{-1}6a_g^{-1}2a_u^{-1}, 1b_{2g}^{-1}3b_{1u}^{-1}4b_{1u}^{-1})$	$A_g$	264.34	0.35	spectator
$^2B_{3u}(3b_{3u}^{-1}, 1b_{3g}^{-1}3b_{1u}^{-1}4b_{1u}^{-1}, 1b_{3g}^{-1}6a_g^{-1}2a_u^{-1})$	$B_{1g}$	264.34	0.16	spectator
$^2B_{2u}(1b_{3g}^{-1}8b_{2u}^{-1}, 1b_{3g}^{-1}5b_{2u}^{-1}, 1b_{3g}^{-1}7b_{1u}^{-1})$	$A_g$	263.55	0.52	spectator
$^2B_{3u}(1b_{2g}^{-1}9b_{3u}^{-1}, 1b_{2g}^{-1}6b_{3u}^{-1}, 1b_{2g}^{-1}8b_{3u}^{-1})$	$B_{1g}$	263.55	0.17	spectator

Auger spectrum based on the data in Table 2. This helps to anticipate the different character of the channels in different energy regimes. The higher Auger electron energy regime has contributions mostly from participator decay channels formed by the ionization of outer valence orbitals. As we move toward lower Auger electron energy, peaks that mostly stem from spectator decay appear. The spectator decay channels ( $2h1p$  channels) are not well described by EOM-IP-CCSD. Hence, we anticipate that this part of the spectrum is not well

described and that some account of triple excitations is needed for these states.

Figure 7 shows the theoretical Auger spectrum of the  $^1B_{1u}$  core-excited state at 285.83 eV compared with the experimental spectrum<sup>56</sup> taken around the  $1s_C \rightarrow \pi^*$  resonance at 285 eV. The peaks in the theoretical spectrum above 270 eV appear exclusively due to participator decay, and their positions agree well with the experimental spectrum. The peaks between 270 and 265 eV have contributions from both participator and

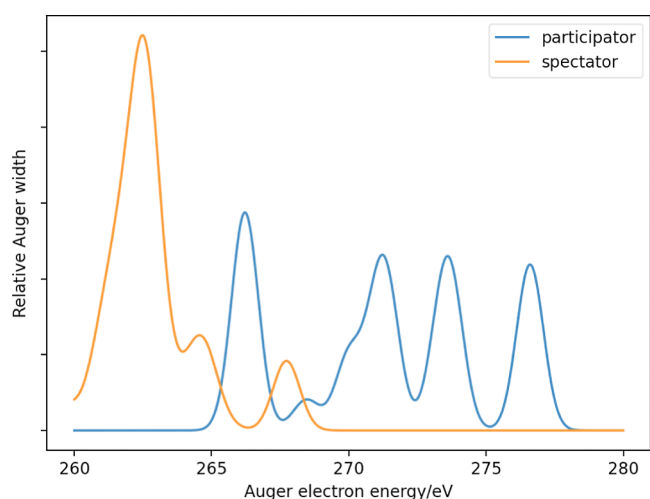


**Figure 6.** Contributions from participator and spectator decay channels to the resonant Auger spectrum of the core-excited  ${}^1B_{1u}$  state of benzene at 285.83 eV.

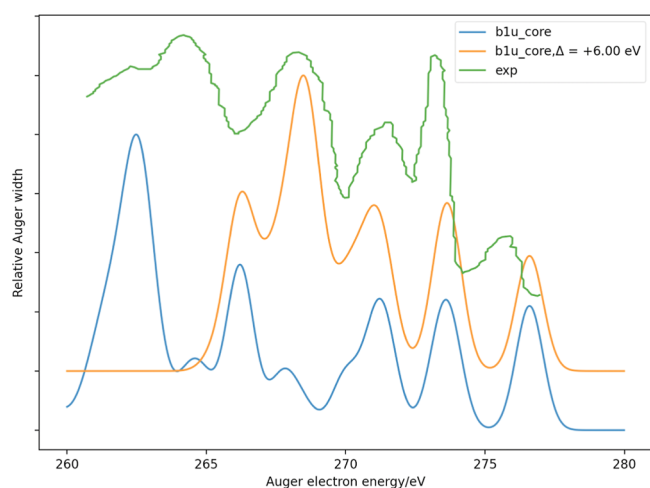


**Figure 7.** Computed resonant Auger spectrum for the core-excited  ${}^1B_{1u}$  state at 285.83 eV along with the experimental spectrum by Rennie et al.<sup>56</sup> A spectrum in which the energies of all  $2h1p$  channels are shifted by 6.00 eV to higher energy is also shown.

spectator decay channels, whereas the remaining peaks with Auger electron energies below 265 eV arise exclusively from spectator decay. The agreement between theory and experiment in terms of the position and intensity of the peaks is rather poor in this energy range. This can be attributed to the poor description of  $2h1p$  states by EOM-IP CCSD.

Figure 7 also shows a spectrum in which an empirical redshift of +6.00 eV is applied to the Auger electron energy of all spectator decay channels to maximize the alignment. We note that 6 eV is a rather substantial redshift of the valence IEs. In the Supporting Information (Figure S2), we show spectra with other values of the shifts, illustrating that smaller shifts result in worse alignment.

Although after applying the global 6 eV shift, the theoretical spectrum aligns better with the experiment, both in terms of the number of peaks and their positions, substantial disagreement persists. Inclusion of triple excitations, which shifts each peak by a different energy, is clearly needed to improve the description of  $2h1p$  states and their signatures in the Auger spectrum.

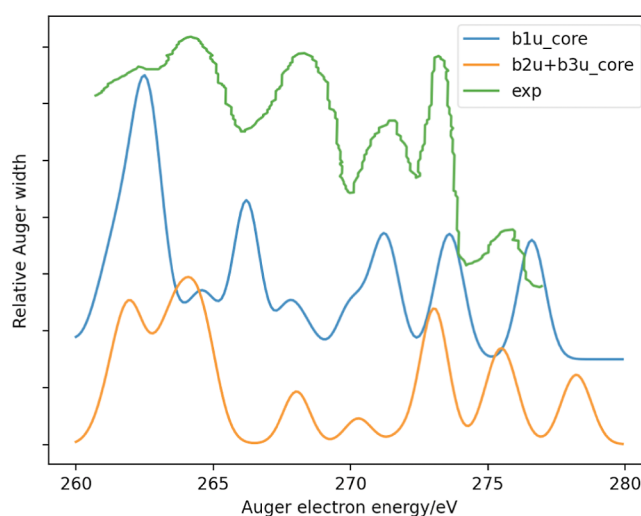


**Figure 8.** Theoretical Auger spectrum of the core-excited  $B_{1u}$  and  $B_{2u}/B_{3u}$  states compared with the spectrum measured by Rennie et al.<sup>56</sup> at 285 eV.

To better understand the effect of the initially excited state, we also computed the resonant Auger spectrum of the  $B_{2u}/B_{3u}$  core-excited state. Figure 8 compares the spectra of the  $B_{1u}$  and  $B_{2u}/B_{3u}$  states; the experimental spectrum is also shown. We observe that the  $B_{1u}$  and  $B_{2u}/B_{3u}$  spectra are noticeably different. As anticipated, the  $B_{1u}$  spectrum matches the experimental spectrum much better. However, it is not clear whether the experimental spectrum also contains contributions from the  $B_{2u}/B_{3u}$  state due to insufficient spectral resolution. If this is the case, these additional contributions could explain the observed discrepancies between theory and experiment, for example, the peak at around 273 eV in the experimental spectrum.

**3.6. Improving the Description of the Decay Channels by Including Triples Corrections.** Table 4 presents the IEs of the decay channels computed using two different noniterative methods for the approximate treatment of triple excitations on top of EOM-CCSD, namely, EOM-IP-CCSD(T)(a)\* and EOM-IP-CCSD(fT) (see Section 2). In the case of  $1h$  states, the magnitude of the triples correction is less than 0.5 eV. Figure 9 shows the participator decay spectrum of the core-excited  $B_{1u}$  and  $B_{2u}/B_{3u}$  states obtained from EOM-IP-CCSD and EOM-CCSD(T)(a)\* calculations. It is evident that the participator decay channels are well described at the EOM-IP-CCSD level of theory.

As expected, the magnitude of the triples correction is much larger for the spectator decay channels (that is, the  $2h1p$  states), ranging between 3 and 6 eV. We were not able to compute all required  $2h1p$  states with EOM-CCSD(T)(a)\*, but we were able to compute the correction for all spectator decay channels with EOM-CCSD(fT). Figure 10 shows the total resonant Auger spectrum of the  ${}^1B_{1u}$  state computed with and without the (fT) correction. The improvement in the relative position of the peaks due to the (fT) correction is clearly visible, but there is a stark disparity between experiment and theory in the intensity of the peak around 275 eV. As we expect participator decay to be more important than spectator decay in this energy range, the discrepancy might be due to contributions of other core-excited states such as the  ${}^1B_{2u}/{}^1B_{3u}$  state (peak B in the XAS).

**Table 4. Ionization Energies of the Lowest Ionized States of Benzene Computed with Different EOM-IP-CC Methods<sup>a</sup>**

state	EOM-CCSD/u6-311(2+,+)G**	(T)(a)* /6-311(+ )G*	(T)(a)* /u6-311(2+,+)G**	(fT) /u6-311(2+,+)G**
<sup>2</sup> B <sub>2g</sub> / <sup>2</sup> B <sub>3g</sub>	9.23	-0.06	-0.02	-0.23
<sup>2</sup> A <sub>g</sub> / <sup>2</sup> B <sub>1g</sub>	12.12	-0.12	-0.10	-0.19
<sup>2</sup> B <sub>1u</sub>	12.55	-0.38	-0.24	-0.34
<sup>2</sup> B <sub>2u</sub> / <sup>2</sup> B <sub>3u</sub>	14.41	-0.14	-0.13	-0.20
<sup>2</sup> B <sub>2u</sub>	14.82	-0.22	-0.21	-0.30
<sup>2</sup> B <sub>3u</sub>	15.83	-0.18	-0.17	-0.21
<sup>2</sup> A <sub>g</sub>	17.38	-0.25	-0.24	-0.27
<sup>2</sup> A <sub>g</sub> / <sup>2</sup> B <sub>1g</sub>	19.62	-0.36	-0.36	-0.38
<sup>2</sup> A <sub>u</sub> / <sup>2</sup> B <sub>1u</sub>	17.56	-3.36	-3.04	-3.60
<sup>2</sup> A <sub>u</sub> / <sup>2</sup> B <sub>1u</sub>	18.10	-5.01	-3.42	-3.43
<sup>2</sup> A <sub>u</sub> / <sup>2</sup> B <sub>1u</sub>	20.27	-5.42	-5.09	-4.94
<sup>2</sup> B <sub>3g</sub>	19.88	-5.14		-3.10
<sup>2</sup> B <sub>2g</sub>	20.00	-5.37		-3.37
<sup>2</sup> B <sub>2u</sub> / <sup>2</sup> B <sub>3u</sub>	20.55	-4.26		-3.94
<sup>2</sup> B <sub>1u</sub>	21.61	-4.58		-5.65

<sup>a</sup>Absolute ionization energies are given for EOM-IP-CCSD and corrections relative to EOM-IP-CCSD for EOM-IP-CCSD(T)(a)\* and EOM-IP-CCSD(fT).

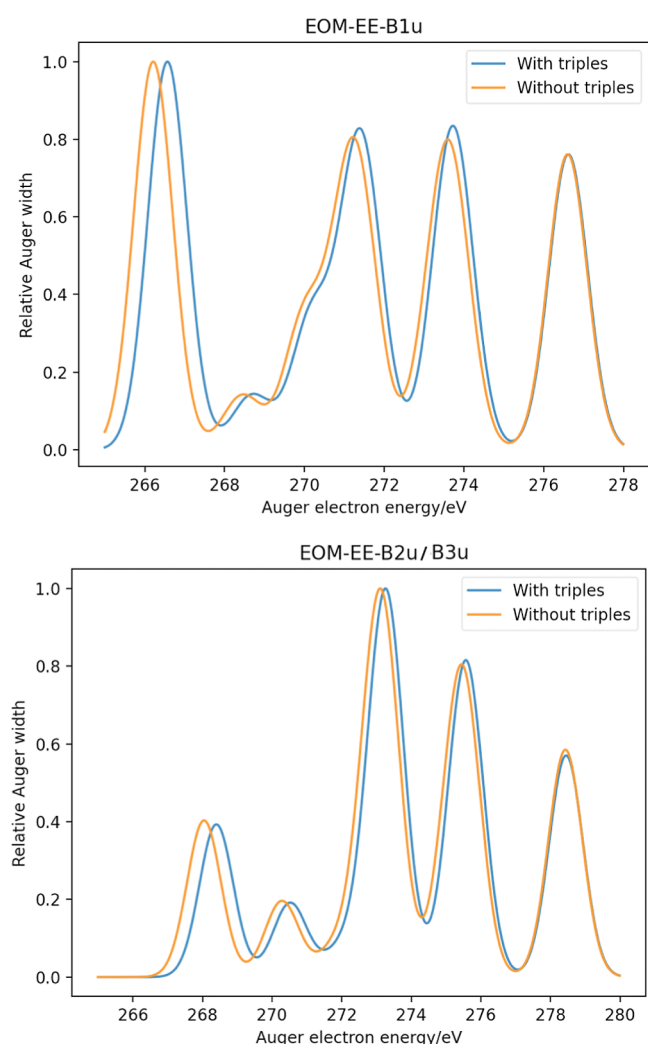


**Figure 9.** Participator decay Auger spectrum computed using EOM-IP-CCSD and EOM-IP-CCSD(T)(a)\* for the decay channels. Top panel: Decay from <sup>1</sup>B<sub>1u</sub> state; Bottom panel: Decay from <sup>1</sup>B<sub>2u</sub>/<sup>1</sup>B<sub>3u</sub> state.

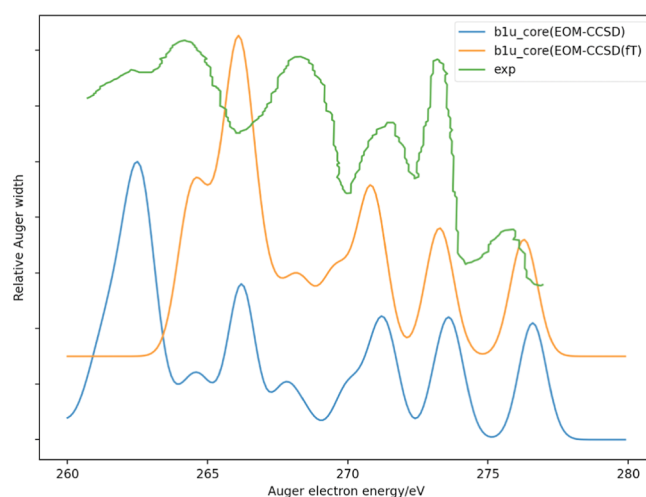


**Figure 10.** Resonant Auger spectrum of the core-excited <sup>1</sup>B<sub>1u</sub> state computed using EOM-IP-CCSD and EOM-IP-CCSD(fT) for the decay channels.

Table 4 compares the IEs computed with EOM-CCSD and EOM-CCSD(T)(a)\* in the 6-311(+ )G\* basis set. In this smaller basis set, we could calculate a larger number of spectator decay channels. Similar to the calculations in the larger basis set, the triples correction for spectator decay channels ranges between 3 and 6 eV.

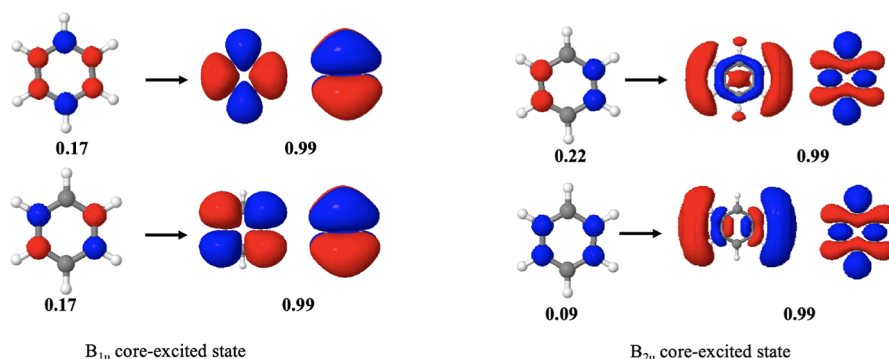
Figure S9 in the Supporting Information compares the spectra computed with EOM-IP-CCSD and with inclusion of triples correction. Here, we shifted the EOM-IP-CCSD energies calculated in the u6-311(2+,+)G\*\* basis using the EOM-IP-CCSD(T)(a)\* triples correction calculated in the smaller 6-311(+ )G\* basis. We note that the (fT) and (T)(a)\* corrections computed with the smaller basis are similar in magnitude.

This analysis shows that the magnitude of triples correction for the *2h1p* states can indeed reach 6 eV. With such a large correction, the accuracy of a perturbative treatment becomes questionable. Hence, for the reliable modeling of resonant Auger spectra, inclusion of triple excitations in an iterative fashion might be necessary. Moreover, the perturbative triples

**Table 5.** Comparison between EOM-IP-CCSD Energies of  $2h1p$  States and EOM-DIP-CCSD Energies of  $2h$  States Computed in the  $u6-311(2+,+)G^{**}$  Basis

state	EOM-IP-CCSD	state	EOM-DIP-CCSD	EOM-DIP-CCSD, shifted <sup>a</sup>
$^2A_u/{}^2B_{1u}$	17.56	${}^3B_{1g}$	24.85	19.64
$^2A_u/{}^2B_{1u}$	18.10	${}^1A_g/{}^1B_{1g}$	25.48	20.27
$^2A_u/{}^2B_{1u}$	20.27	${}^1A_g/{}^1B_{1g}$	25.48	20.27
${}^2B_{2g}/{}^2B_{3g}$	21.45	${}^3B_{2u}/{}^3B_{3u}$	27.90	22.69

<sup>a</sup>EOM-DIP-CCSD energy minus lowest  $\pi\pi^*$  singlet excitation energy of benzene computed with EOM-EE-CCSD/ $u6-311(2+,+)G^{**}$ .

**Figure 11.** Natural Auger orbitals for participator Auger decay in benzene. Left: Decay of the core-excited  ${}^1B_{1u}$  state into the  ${}^2B_{1g}$  state. Right: Decay of the core-excited  ${}^1B_{2u}$  state into the  ${}^2A_g$  state.

corrections only affect the peak positions while the decay widths are computed based on EOM-IP-CCSD wave functions. Given the large magnitude of the energy correction, one may anticipate large changes in the amplitudes due to triples, which, translated into the changes in two-body Dyson orbitals, may lead to nontrivial effects of explicit triple excitations on the decay widths.

**3.7. Describing the Spectator Decay Channels with EOM-DIP-CCSD.** Anticipating the poor description of the  $2h1p$  states by EOM-IP-CCSD, we also carried out EOM-DIP-CCSD calculations. The energies of the  $2h$  states, shifted by the lowest  $\pi\pi^*$  singlet excitation energy, which amounts to 5.21 eV computed with EOM-EE-CCSD ( ${}^1B_{2u}$ ), can provide estimates for the IEs of the  $2h1p$  states, assuming that the excited spectator electron is relatively far away and interacts only weakly with the molecular core.<sup>80</sup> While it is clear that such treatment of problematic  $2h1p$  states is not perfect, it provides an alternative estimate for the spectator decay channels. We expect that such estimate provides an upper bound to the  $2h1p$  EOM-IP states.

Table 5 compares the  $2h$  EOM-DIP-CCSD states and the  $2h1p$  EOM-IP-CCSD states. To match the DIP and IP states, we compare the respective leading electronic configurations. We note that sometimes the best match is achieved for DIP singlets and sometimes for the DIP triplets. As one can see, the DIP states follow the same ordering as the IP states, with their shifted energies being  $\sim 2$  eV higher. Hence, one can use DIP calculations to represent  $2h1p$  IP states, but an additional empirical shift is needed to match the energies.

**3.8. Natural Auger Orbitals.** To better understand the contributions of resonant decay to the Auger spectrum of benzene, we computed natural Auger orbitals (NAOs)<sup>81</sup> for different core-excited states and decay channels. Figure 11 shows the participator decay NAOs for the  $B_{1u}$  and  $B_{2u}/B_{3u}$  core-excited states.

NAOs provide information about the initial core-excited state and the final decay channels, which are the  $1h$  states in

the case of participator decay. Thus, NAOs are useful for examining the orbital picture associated with each decay channel. For instance, from Figure 11, it is evident that the decay of the  $B_{1u}$  core-excited state creates a hole in the  $2a_g$  and  $1b_{1g}$  core orbitals. The initially excited electron populates the one of the LUMOs ( $4b_{1u}$  or  $2a_u$ ), which, in turn, takes part in resonant Auger decay, thereby ejecting the Auger electron from the corresponding HOMOs of benzene ( $1b_{2g}$  and  $1b_{3g}$ ). The degenerate  ${}^1B_{2u}/{}^1B_{3u}$  core-excited states generate holes in the  $1b_{2u}/1b_{3u}$  orbitals and in  $1a_g/2a_g$  orbitals. Figure 11 indeed shows that the  $B_{2u}$  core excitation corresponds to a  $1s_C$  to Rydberg orbitals transition and the removal of the Auger electron from the  $6a_g$  orbital (HOMO - 1).

## 4. CONCLUSIONS

We presented calculations of the resonant Auger spectrum of benzene using the Feshbach–Fano approach combined with EOM-CCSD wave functions and a description of the Auger electron in terms of plane waves. The calculations reproduce well the higher-energy part of the experimental Auger spectrum, which is dominated by participator decay. The lower-energy part of the spectrum, which includes contributions from spectator decay, shows large discrepancies with experiment.

This shortcoming is anticipated because the spectator decay channels are dominated by  $2h1p$  configurations that are not well described by EOM-IP-CCSD. To improve the description of this part of the spectrum, we investigated several approaches: an empirical redshift of all  $2h1p$  states by 6 eV, two types of noniterative triples corrections on top of EOM-IP-CCSD, as well as using EOM-DIP-CCSD energies shifted by the lowest  $\pi\pi^*$  excitation energy of benzene. The so-corrected spectra agree better with experiment, but discrepancies still persist. The two triples corrections are in good agreement with each other; however, given the large magnitude of the correction of up to 6 eV, one may expect that a perturbative noniterative treatment is not sufficient and



that an iterative inclusion of triple excitations is needed instead.

Furthermore, the triples corrections only affect the peak positions while the decay widths are still computed based on EOM-IP-CCSD wave functions. One may anticipate nontrivial effects of triple excitations on the decay widths, which can affect the spectrum. It is also not clear whether the available experiment can reliably isolate the spectra arising from resonant Auger decay of different core-excited states. The X-ray absorption spectrum of benzene is dominated by a  $1s_C \rightarrow \pi^*$  transition at 285 eV, but there are other core-excited states just a few electron-volts higher. Our results show that the Auger spectra resulting from excitations to the two lowest-lying peaks in the X-ray absorption spectrum are different, meaning that one may anticipate considerable changes in the resonant Auger spectrum if the two peaks are not spectrally resolved. Finally, given the large discrepancies between different experimental nonresonant Auger spectra of benzene,<sup>54</sup> one cannot rule out the possibility that the experimental resonant spectrum might be affected by some artifacts.

## ■ ASSOCIATED CONTENT

### Data Availability Statement

The data that support the findings of this study are available within the article and the associated [Supporting Information](#).

### SI Supporting Information

The Supporting Information is available free of charge at <https://pubs.acs.org/doi/10.1021/acs.jpca.4c07304>.

Relevant Cartesian geometries; input details; additional results for XAS and Auger spectra ([PDF](#))

## ■ AUTHOR INFORMATION

### Corresponding Author

Anna I. Krylov – Department of Chemistry, University of Southern California, Los Angeles, California 90089, United States; [orcid.org/0000-0001-6788-5016](https://orcid.org/0000-0001-6788-5016);  
Email: [krylov@usc.edu](mailto:krylov@usc.edu)

### Authors

Nayanthara K. Jayadev – Department of Chemistry, University of Southern California, Los Angeles, California 90089, United States; [orcid.org/0000-0003-1174-5668](https://orcid.org/0000-0003-1174-5668)

Thomas-C. Jagau – Department of Chemistry, KU Leuven, B-3001 Leuven, Belgium; [orcid.org/0000-0001-5919-424X](https://orcid.org/0000-0001-5919-424X)

Complete contact information is available at: <https://pubs.acs.org/doi/10.1021/acs.jpca.4c07304>

### Notes

The authors declare the following competing financial interest(s): A.I.K. is the president and a part-owner of Q-Chem, Inc.

## ■ ACKNOWLEDGMENTS

This work was supported in Los Angeles by the U.S. National Science Foundation (no. CHE-2154482 to A.I.K.) and in Leuven by the European Research Council (ERC) under the European Union's Horizon 2020 research and innovation program (Grant no. 851766 to T.C.J.) and by the KU Leuven internal funds (Grant no. C14/22/083 to T.C.J.).

## ■ REFERENCES

- (1) Agarwal, B. K. *X-ray spectroscopy: An introduction, volume 15*; Springer, 2013.
- (2) Orvis, T.; Surendran, M.; Liu, Y.; Cunniff, A.; Ravichandran, J. In situ Auger electron spectroscopy of complex oxide surfaces grown by pulsed laser deposition. *J. Vac. Sci. Technol., A* **2019**, *37*, 061401.
- (3) Weightman, P. *Electronic Properties of Surfaces, Chapter X-ray-excited Auger and photoelectron spectroscopy*; Routledge: New York, 1984; pp 135–195.
- (4) Li, Z.; Becker, U. Chemical state effects on the Auger transitions in Cr, Fe, and Cu compounds. *J. Electron Spectrosc. Relat. Phenom.* **2019**, *237*, 146893.
- (5) Hofmann, S. *Auger- and X-ray photoelectron spectroscopy in materials science: A user-oriented guide*; Springer Science & Business Media, 2012; Vol. 49.
- (6) Chao, L.-C.; Yang, S.-H. Growth and Auger electron spectroscopy characterization of donut-shaped ZnO nanostructures. *Appl. Surf. Sci.* **2007**, *253*, 7162.
- (7) Raman, S. N.; Paul, D. F.; Hammond, J. S.; Bomben, K. D. Auger electron spectroscopy and its application to nanotechnology. *Microsc. Today* **2011**, *19*, 12.
- (8) Unger, W. E. S.; Wirth, T.; Hodoroaba, V.-D. Chapter 4.3.2 - Auger electron spectroscopy. In *Characterization of Nanoparticles*; Elsevier, 2020; pp 373–395.
- (9) Rye, R. R.; Houston, J. E. Molecular Auger spectroscopy. *Acc. Chem. Res.* **1984**, *17*, 41.
- (10) McFarland, B. K.; Farrell, J. P.; Miyabe, S.; Tarantelli, F.; Aguilar, A.; Berrah, N.; Bostedt, C.; Bozek, J. D.; Bucksbaum, P. H.; Castagna, J. C.; et al. Ultrafast x-ray Auger probing of photoexcited molecular dynamics. *Nat. Commun.* **2014**, *5*, 4235.
- (11) Marchenko, T.; Inhester, L.; Goldsztejn, G.; Travnikova, O.; Journal, L.; Guillemin, R.; Ismail, I.; Koulentianos, D.; Céolin, D.; Püttner, R.; et al. Ultrafast nuclear dynamics in the doubly-core-ionized water molecule observed via Auger spectroscopy. *Phys. Rev. A* **2018**, *98*, 063403.
- (12) Plekan, O.; Sa'adeh, H.; Ciavardini, A.; Callegari, C.; Cautero, G.; Dri, C.; Di Fraia, M.; Prince, K. C.; Richter, R.; Sergo, R.; et al. Experimental and theoretical photoemission study of indole and its derivatives in the gas phase. *J. Phys. Chem. A* **2020**, *124*, 4115.
- (13) Ku, A.; Facca, V. J.; Cai, Z.; Reilly, R. M. Auger electrons for cancer therapy – a review. *EJNMMI radiopharm. chem.* **2019**, *4*, 27.
- (14) Pirovano, G.; Jannetti, S. A.; Carter, L. M.; Sadique, A.; Kossatz, S.; Guru, N.; Demétrio De Souza França, P.; Maeda, M.; Zeglis, B. M.; Lewis, J. S.; et al. Targeted brain tumor radiotherapy using an Auger emitter. *Clin. Cancer Res.* **2020**, *26*, 2871.
- (15) Borbinha, J.; Vaz, P.; Di Maria, S. Dosimetric assessment in different tumour phenotypes with Auger electron emitting radionuclides: <sup>99m</sup>Tc, <sup>125</sup>I, <sup>161</sup>Tb, and <sup>177</sup>Lu. *Radiat. Phys. Chem.* **2020**, *172*, 108763.
- (16) Pirovano, G.; Wilson, T. C.; Reiner, T. Auger: The future of precision medicine. *Nucl. Med. Biol.* **2021**, *96*, 50.
- (17) Kassis, A. I. The amazing world of Auger electrons. *Int. J. Radiat. Biol.* **2004**, *80*, 789.
- (18) Tarantelli, F.; Sgamellotti, A.; Cederbaum, L. S.; Schirmer, J. Theoretical investigation of many dicationic states and the Auger spectrum of benzene. *J. Chem. Phys.* **1987**, *86*, 2201.
- (19) Ohrendorf, E. M. L.; Tarantelli, F.; Cederbaum, L. S. Dicationic states of hydrocarbons and a statistical approach to their Auger spectra. *J. Chem. Phys.* **1990**, *92*, 2984–2999.
- (20) Fano, U. Effects of configuration interaction on intensities and phase shifts. *Phys. Rev.* **1961**, *124*, 1866.
- (21) Feshbach, H. A unified theory of nuclear reactions. 2. *Ann. Phys.* **1962**, *19*, 287.
- (22) Löwdin, P.-O. Studies in perturbation theory. IV. Solution of eigenvalue problem by projection operator formalism. *J. Math. Phys.* **1962**, *3*, 969.
- (23) Cederbaum, L. S.; Domcke, W.; Schirmer, J. Many-body theory of core holes. *Phys. Rev. A* **1980**, *22*, 206.

- (24) Coriani, S.; Koch, H. Communication: X-ray absorption spectra and core-ionization potentials within a core-valence separated coupled cluster framework. *J. Chem. Phys.* **2015**, *143*, 181103.
- (25) Vidal, M. L.; Feng, X.; Epifanovsky, E.; Krylov, A. I.; Coriani, S. A new and efficient equation-of-motion coupled-cluster framework for core-excited and core-ionized states. *J. Chem. Theory Comput.* **2019**, *15*, 3117.
- (26) Vidal, M. L.; Krylov, A. I.; Coriani, S. Dyson orbitals within the fc-CVS-EOM-CCSD framework: theory and application to X-ray photoelectron spectroscopy of ground and excited states. *Phys. Chem. Chem. Phys.* **2020**, *22*, 2693.
- (27) Vidal, M. L.; Krylov, A. I.; Coriani, S. Correction to: "Dyson orbitals within the fc-CVS-EOM-CCSD framework: Theory and application to X-ray photoelectron spectroscopy of ground and excited states. *Phys. Chem. Chem. Phys.* **2020**, *22*, 3744.
- (28) Liegener, C.-M. Green's function calculations on the Auger spectra of CO. *Chem. Phys. Lett.* **1984**, *106*, 201.
- (29) Carravetta, V.; Ågren, H. Stieltjes imaging method for molecular Auger transition rates: Application to the Auger spectrum of water. *Phys. Rev. A* **1987**, *35*, 1022–1032.
- (30) Dreuw, A.; Wormit, M. The algebraic diagrammatic construction scheme for the polarization propagator for the calculation of excited states. *Wiley Interdiscip. Rev.: Comput. Mol. Sci.* **2015**, *5*, 82.
- (31) Averbukh, V.; Cederbaum, L. S. Ab initio calculation of interatomic decay rates by a combination of the Fano ansatz, Green's-function methods, and the Stieltjes imaging technique. *J. Chem. Phys.* **2005**, *123*, 204107.
- (32) Kopelke, S.; Gokhberg, K.; Cederbaum, L. S.; Tarantelli, F.; Averbukh, V. Autoionization widths by Stieltjes imaging applied to Lanczos pseudospectra. *J. Chem. Phys.* **2011**, *134*, 024106.
- (33) Kolorenč, P.; Averbukh, V. Fano-ADC(2,2) method for electronic decay rates. *J. Chem. Phys.* **2020**, *152*, 214107.
- (34) Kolorenč, P. Ab initio calculations of molecular double Auger decay rates. *J. Chem. Phys.* **2024**, *161*, 174102.
- (35) Siegbahn, H.; Asplund, L.; Kelfve, P. The Auger electron spectrum of water vapour. *Chem. Phys. Lett.* **1975**, *35*, 330.
- (36) Fink, R. F.; Piancastelli, M. N.; Grum-Grzhimailo, A. N.; Ueda, K. Angular distribution of Auger electrons from fixed-in-space and rotating C 1s  $\rightarrow$  2 $\pi$  photoexcited CO: Theory. *J. Chem. Phys.* **2009**, *130*, 014306.
- (37) Grell, G.; Bokarev, S. I. Multi-reference protocol for (auto) ionization spectra: Application to molecules. *J. Chem. Phys.* **2020**, *152*, 074108.
- (38) Tenorio, B. N. C.; Voß, T. A.; Bokarev, S. I.; Declava, P.; Coriani, S. Multi-reference approach to normal and resonant Auger spectra based on the one-center approximation. *J. Chem. Theory Comput.* **2022**, *18*, 4387–4407.
- (39) Grell, G.; Kühn, O.; Bokarev, S. I. Multireference quantum chemistry protocol for simulating autoionization spectra: Test of ionization continuum models for the neon atom. *Phys. Rev. A* **2019**, *100*, 042512.
- (40) Inhester, L.; Burmeister, C. F.; Groenhof, G.; Grubmüller, H. Auger spectrum of a water molecule after single and double core ionization. *J. Chem. Phys.* **2012**, *136*, 144304.
- (41) Demekhin, P. V.; Cederbaum, L. S. Strong interference effects in the resonant Auger decay of atoms induced by intense x-ray fields. *Phys. Rev. A* **2011**, *83*, 023422.
- (42) Demekhin, P. V.; Cederbaum, L. S. Resonant Auger decay of core-excited CO molecules in intense x-ray laser pulses: The O(1s  $\rightarrow$   $\pi^*$ ) excitation. *J. Phys. B: At., Mol. Opt. Phys.* **2013**, *46*, 164008.
- (43) Skomorowski, W.; Krylov, A. I. Feshbach-Fano approach for calculation of Auger decay rates using equation-of-motion coupled-cluster wave functions. I. Theory and implementation. *J. Chem. Phys.* **2021**, *154*, 084124.
- (44) Rescigno, T. N.; McCurdy, C. W.; Orel, A. E. Extensions of the complex-coordinate method to the study of resonances in many-electron systems. *Phys. Rev. A* **1978**, *17*, 1931.
- (45) White, A. F.; Head-Gordon, M.; McCurdy, C. W. Complex basis functions revisited: Implementation with applications to carbon tetrafluoride and aromatic N-containing heterocycles within the static-exchange approximation. *J. Chem. Phys.* **2015**, *142*, 054103.
- (46) Matz, F.; Jagau, T.-C. Channel-specific core-valence projectors for determining partial Auger decay widths. *Mol. Phys.* **2022**, *121*, No. e2105270.
- (47) Matz, F.; Jagau, T.-C. Molecular Auger decay rates from complex-variable coupled-cluster theory. *J. Chem. Phys.* **2022**, *156*, 114117.
- (48) Krylov, A. I. Equation-of-motion coupled-cluster methods for open-shell and electronically excited species: The hitchhiker's guide to Fock space. *Annu. Rev. Phys. Chem.* **2008**, *59*, 433.
- (49) Skomorowski, W.; Krylov, A. I. Feshbach-Fano approach for calculation of Auger decay rates using equation-of-motion coupled-cluster wave functions. II. Numerical examples and benchmarks. *J. Chem. Phys.* **2021**, *154*, 084125.
- (50) Matz, F.; Nijssen, J.; Jagau, T.-C. Ab initio investigation of the Auger spectra of methane, ethane, ethylene, and acetylene. *J. Phys. Chem. A* **2023**, *127*, 6147.
- (51) Parravicini, V.; Jagau, T.-C. Interatomic and intermolecular Coulombic decay rates from equation-of-motion coupled-cluster theory with complex basis functions. *J. Chem. Phys.* **2023**, *159*, 094112.
- (52) Drennhaus, J. P.; Ferino-Pérez, A.; Matz, F.; Jagau, T.-C. Ab initio treatment of molecular Coster-Kronig decay using complex-scaled equation-of-motion coupled-cluster theory. *Phys. Chem. Chem. Phys.* **2024**, *26*, 23846.
- (53) Ferino-Pérez, A.; Jagau, T.-C. Ab initio computation of Auger decay in heavy metals: Zinc about it. *J. Phys. Chem. A* **2024**, *128*, 3957.
- (54) Jayadev, N. K.; Ferino-Pérez, A.; Matz, F.; Krylov, A. I.; Jagau, T.-C. The Auger spectrum of benzene. *J. Chem. Phys.* **2023**, *158*, 064109.
- (55) Spohr, R.; Bergmark, T.; Magnusson, N.; Werme, L. O.; Nordling, C.; Siegbahn, K. Electron spectroscopic investigation of Auger processes in bromine substituted methanes and some hydrocarbons. *Phys. Scr.* **1970**, *2*, 31.
- (56) Rennie, E. E.; Kempgens, B.; Köppe, H. M.; Hergenbahn, U.; Feldhaus, J.; Itchkawitz, B. S.; Kilcoyne, A. L. D.; Kivimäki, A.; Maier, K.; Piancastelli, M. N.; et al. A comprehensive photoabsorption, photoionization, and shake-up excitation study of the C1s cross section of benzene. *J. Chem. Phys.* **2000**, *113*, 7362.
- (57) Carniato, S.; Selles, P.; Ferté, A.; Berrah, N.; Wuosmaa, A. H.; Nakano, M.; Hikosaka, Y.; Ito, K.; Žitnik, M.; Bučar, K.; et al. Single photon simultaneous K-shell ionization/excitation in C<sub>6</sub>H<sub>6</sub>: Experiment and theory. *J. Phys. B: At., Mol. Opt. Phys.* **2020**, *53*, 244010.
- (58) Manohar, P. U.; Krylov, A. I. A non-iterative perturbative triples correction for the spin-flipping and spin-conserving equation-of-motion coupled-cluster methods with single and double substitutions. *J. Chem. Phys.* **2008**, *129*, 194105.
- (59) Manohar, P. U.; Stanton, J. F.; Krylov, A. I. Perturbative triples correction for the equation-of-motion coupled-cluster wave functions with single and double substitutions for ionized states: Theory, implementation, and examples. *J. Chem. Phys.* **2009**, *131*, 114112.
- (60) Matthews, D. A.; Stanton, J. F. A new approach to approximate equation-of-motion coupled cluster with triple excitations. *J. Chem. Phys.* **2016**, *145*, 124102.
- (61) Jagau, T. C. Non-iterative triple excitations in equation-of-motion coupled-cluster theory for electron attachment with applications to bound and temporary anions. *J. Chem. Phys.* **2018**, *148*, 024104.
- (62) Sarangi, R.; Vidal, M. L.; Coriani, S.; Krylov, A. I. On the basis set selection for calculations of core-level states: Different strategies to balance cost and accuracy. *Mol. Phys.* **2020**, *118*, No. e1769872.
- (63) Vidal, M. L.; Epshtein, M.; Scutelnic, V.; Yang, Z.; Xue, T.; Leone, S. R.; Krylov, A. I.; Coriani, S. The interplay of open-shell spin-coupling and Jahn–Teller distortion in benzene radical cation probed by x-ray spectroscopy. *J. Phys. Chem. A* **2020**, *124*, 9532.

(64) Epifanovsky, E.; Gilbert, A. T. B.; Feng, X.; Lee, J.; Mao, Y.; Mardirossian, N.; Pokhilko, P.; White, A. F.; Coons, M. P.; Dempwolff, A. L.; et al. Software for the frontiers of quantum chemistry: An overview of developments in the Q-Chem 5 package. *J. Chem. Phys.* **2021**, *155*, 084801.

(65) Krylov, A. I.; Gill, P. M. W. Q-Chem: An engine for innovation. *Wiley Interdiscip. Rev.:Comput. Mol. Sci.* **2013**, *3*, 317.

(66) Mulliken, R. S. Report on notation for the spectra of polyatomic molecules. *J. Chem. Phys.* **1955**, *23*, 1997.

(67) Depending on molecular orientation, symmetry labels corresponding to the same orbital or vibrational mode may be different. Q-Chem's standard molecular orientation is different from that of Mulliken.<sup>66</sup> For example, Q-Chem would place water molecule in the *xz* plane instead of the *yz*. Consequently, for  $C_{2v}$  symmetry,  $b_1$  and  $b_2$  labels are flipped. More details can be found at <http://iopenshell.usc.edu/resources/howto/symmetry/>. To avoid confusion with different molecular orientations and relabeling the states, here we report the structures and symmetry labels following the Q-Chem's notations.

(68) Nanda, K. D.; Vidal, M. L.; Faber, R.; Coriani, S.; Krylov, A. I. How to stay out of trouble in RIXS calculations within the equation-of-motion coupled-cluster damped response theory? Safe hitchhiking in the excitation manifold by means of core-valence separation. *Phys. Chem. Chem. Phys.* **2020**, *22*, 2629.

(69) Nanda, K. D.; Vidal, M. L.; Faber, R.; Coriani, S.; Krylov, A. I. Correction: "How to stay out of trouble in RIXS calculations within the equation-of-motion coupled-cluster damped response theory? Safe hitchhiking in the excitation manifold by means of core-valence separation. *Phys. Chem. Chem. Phys.* **2020**, *22*, 17749.

(70) Mewes, S. A.; Plasser, F.; Krylov, A.; Dreuw, A. Benchmarking excited-state calculations using exciton properties. *J. Chem. Theory Comput.* **2018**, *14*, 710.

(71) Plasser, F.; Krylov, A. I.; Dreuw, A. libwfa: Wavefunction analysis tools for excited and open-shell electronic states. *Wiley Interdiscip. Rev.:Comput. Mol. Sci.* **2022**, *12*, No. e1595.

(72) Menzel, D.; Rocker, G.; Steinrück, H.-P.; Heimann, P. A.; Coulmanand, D.; Huber, W.; Zebisch, P.; Lloyd, D. R. Core excitation, decay, and fragmentation in solid benzene as studied by x-ray absorption, resonant Auger, and photon stimulated desorption. *J. Chem. Phys.* **1992**, *96*, 1724.

(73) Epshtein, M.; Scutelnic, V.; Yang, Z.; Xue, T.; Vidal, M. L.; Krylov, A. I.; Coriani, S.; Leone, S. R. Table-top X-ray spectroscopy of benzene radical cation. *J. Phys. Chem. A* **2020**, *124*, 9524.

(74) Little, D. A.; Tennyson, J. An R-matrix study of singlet and triplet continuum states of  $N_2$ . *J. Phys. B:At, Mol. Opt. Phys.* **2014**, *47*, 105204.

(75) Klinker, M.; Marante, C.; Argenti, L.; González-Vázquez, J.; Martín, F. Electron correlation in the ionization continuum of molecules: Photoionization of  $N_2$  in the vicinity of the Hopfield series of autoionizing states. *J. Phys. Chem. Lett.* **2018**, *9*, 756.

(76) Creutzberg, J.; Skomorowski, W.; Jagau, T.-C. Computing decay widths of autoionizing Rydberg states with complex-variable coupled-cluster theory. *J. Phys. Chem. Lett.* **2023**, *14*, 10943.

(77) Ueda, K.; Okunishi, M.; Chiba, H.; Shimizu, Y.; Ohmori, K.; Sato, Y.; Shigemasa, E.; Kosugi, N. Rydberg-valence mixing in the C 1s excited states of  $CH_4$  probed by electron spectroscopy. *Chem. Phys. Lett.* **1995**, *236*, 311.

(78) Neeb, M.; Kivimäki, A.; Kempgens, B.; Köppe, H. M.; Bradshaw, A. M. The C 1s Auger decay spectrum of  $CF_4$ : An analysis of the core-excited states. *J. Phys. B:At, Mol. Opt. Phys.* **1997**, *30*, 93.

(79) Ungier, L.; Thomas, T. D. Near threshold excitation of KVV Auger spectra in carbon monoxide using electron–electron coincidence spectroscopy. *J. Chem. Phys.* **1985**, *82*, 3146.

(80) F., Matz, private communication.

(81) Jayadev, N. K.; Skomorowski, W.; Krylov, A. I. Molecular-orbital framework of two-electron processes: Application to Auger and intermolecular Coulomb decay. *J. Phys. Chem. Lett.* **2023**, *14*, 8612.